**AALBORG
UNIVERSITY**

# Supervisory Control of an Adaptive-Droop Regulated DC Microgrid with Battery Management Capability

Dragicevic, Tomislav; Guerrero, Josep M.; Vasquez, Juan Carlos; Skrlec, Davor

# Supervisory Control of an Adaptive-Droop Regulated DC Microgrid with Battery Management Capability

Tomislav Dragičević, *Student Member, IEEE,* Josep M. Guerrero, *Senior Member, IEEE,* Juan C. Vasquez, *Member, IEEE,* and Davor Škrlec, *Member, IEEE*

*Abstract*—DC power systems are gaining an increasing interest in renewable energy applications because of the good matching with dc output type sources such as photovoltaic (PV) systems and secondary batteries. In this paper, several distributed generators (DGs) have been merged together with a pair of batteries and loads to form an autonomous dc Microgrid (MG). To overcome the control challenge associated with coordination of multiple batteries within one stand-alone MG, a double-layer hierarchical control strategy was proposed; 1) The unit-level primary control layer was established by an adaptive voltage-droop (VD) method aimed to regulate the common bus voltage and to sustain the states of charge (SOCs) of batteries close to each other during moderate replenishment. The control of every unit was expanded with unit-specific algorithm, i.e. finish-of-charging for batteries and maximum power point tracking (MPPT) for renewable energy sources (RESs), with which a smooth on-line overlap was designed; 2) the supervisory control layer was designed to use the low bandwidth communication interface between the central controller and sources in order to collect data needed for adaptive calculation of virtual resistances (VRs) as well as transit criteria for changing unit-level operating modes. A small-signal stability for the whole range of VRs. The performance of developed control was assessed through experimental results.

*Index Terms*—Adaptive droop control, battery charger, distributed generation (DG), Microgrid (MG), supervisory control.

## I. INTRODUCTION

TECHNOLOGICAL advancement in power electronics during the past decade has led to a condition where renewable energy sources (RES) such as wind and photovoltaic (PV) can be virtually considered as completely controllable, within the limits imposed by natural phenomenon [1]. Thus, RES integrated together with other distributed generation (DG) are steadily becoming even competitors in new electricity grids that tend to minimize the consumption of fossil fuels while trying to be more flexible and distributed at the same time.

Objecting to the traditional one way power/information flow, it was conceived that a large-scale integration of new technologies into a smart grid (SG) will be quite difficult if it is done independently. Thus, an idea of merging small

variable nature sources with energy storage system (ESS) into a singular controllable entity that can work autonomously or grid-connected brought to a Microgrid (MG) concept [2]. Depending on the voltage type on common bus, ac and dc MGs can be distinguished. While a lot of work has been done previously in improving the operation of ac MGs [3]–[7], dc MG field has started attracting considerable attention recently, particularly due to a potential of bringing many advantages such as higher efficiency, more natural interface of RES, better compliance with consumer electronics, etc. [8]–[13]. Furthermore, reactive power flow, power quality and frequency control are not an issue in dc systems, making the corresponding primary control notably less complex than its ac version. Currently, most common applications of dc MGs are electrical power supply of isolated systems like vehicles, space crafts, data centers, telecom systems or rural areas [14]–[17].

In both ac and dc applications, tightest control can be achieved if fast intercommunication links between paralleled sources are available. However, with the increasing number of units and/or their spatial diffusion, wiring hardware becomes serious limitation. Moreover, physical differences between converters and lines can trigger the circulating current problem [18]. Hence, to overcome these constraints, a droop control method, taken from traditional power system control [19], has been proposed in both dc and ac MGs [20]. Specifically, the dc MG droop control is usually based on subtracting part of the converter output current proportional to virtual resistance (VR) from voltage reference. Some authors have also proposed multiplication of measured voltage deviation to a value reciprocal to VR [21].

However, it is desirable to extract all available power from RESs, referred to as maximum power point tracking (MPPT) [22], [23], but not always appropriate in isolated systems, as it can lead to an unmanageable excess of energy, resulting in possible overcharging of ESS. On the other hand, a battery, an ESS that is used in this paper, has specific requirements for recharging completion to obtain optimum life [24]. So, there should be an option to control the units in the system according to their specific features as well. For this purpose, a dual control on primary level has been developed in this paper. An attention has been devoted to enable smooth on-line switching between voltage-droop (VD) and unit specific control (MPPT or regulated charging).

The cost of the batteries usually has a big share in the overall cost of isolated systems [25]. Also, their optimal sizing
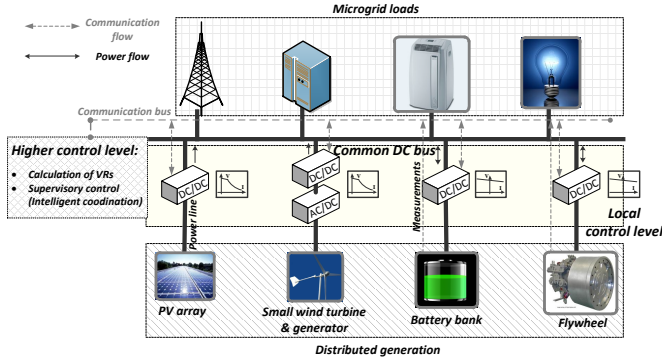
Fig. 1. Diagram of a dc microgrid.

depends on system consumption and production capacity of generating units. Possible increase of consumption within the isolated system will therefore yield a need for storage expansion. Due to hardware limitations, usually the only option to do this is an addition of separate ESS. However, although increased storage capacity gives more flexibility and provides more resilience to prolonged periods without production, its regular re-charging requirements may be too high for small isolated systems with limited power from RESs. As stability of the common bus voltage and its maintenance within acceptable limits should have the highest priority, it is often necessary to distribute the recharging efforts through time. To the best knowledge of the authors, the issue of managing multiple battery stacks within one autonomous system has been out of the scope of most related research up to date. For that purpose, a triple-role supervisory control strategy was developed on top of primary control for a dc MG that consists of RESs and two separate batteries. Its first function includes a novel on-line adaptation of VRs which is designed to achieve asymptotic approaching of batteries' states of charge (SOCs) and is intended for moderate replenishment periods. The second and third function, active at high SOCs, are responsible for distributing the charging and discharging tokens and transitions of operating modes respectively.

The paper is organized as follows. In section II, dc MG configuration is shown and classification of units according to their changing operating states is given. Also, VD control is revised in more detail. Section III provides the ESS modelling and control with the proposal of an adaptive VRs calculation . In Section IV, all details of primary control and functionalities of the supervisory control are revealed. Section V gives a small-signal analysis which is a useful supplement to determine the degree to which VRs can be changed not to compromise the system stability. Experimental results are presented in Section VI in order to validate the feasibility of the proposed approach. Finally, Section VII gives the conclusion.

## II. DC Microgrid Configuration and Control

A dc MG is showed in Fig. 1. It consists of PV and WTG subsystems, two battery banks, a common power bus, a communication link and variety of loads. To achieve parallel operation of diverse sources within the MG, power interfaces

are required in between. They consist of several control stages and associated converters. PV system is made of a PV array and a buck converter. WTG system consists of a small wind turbine and permanent magnet synchronous generator (PMSG) connected to a diode rectifier and buck converter. Both batteries are connected to the common bus through synchronous buck converters to realize bidirectional power flow. DC/DC converters are crucial elements here as they link the common bus with sources and control the current flow between them.

Proposed control structure is divided into two layers; a dual functionality primary control for automatic regulation over current injection into the common bus and a supervisory control for coordination of power generation and provision of specific requirements to the sources using a low-bandwidth communication interface.

Primary control is made of two nested control loops; the outer one responsible for creating a current reference and the inner one which makes sure that the output current follows that reference. Depending on the control strategy incorporated in outer loop, a common classification of units can be made on voltage source converters (VSCs) and current source converters (CSCs). Generally, RESs operating in MPPT mode and batteries during regulated charging act as CSCs as their power injection/extraction does not depend on on-going grid condition. On the other hand, an ability of regulating the coupling point voltage makes VSC units important when forming stand-alone systems. Unlike the traditional approach where only one of these control strategies is applied to a specific unit, all DGs within this MG are able to operate in both VSC and CSC mode and seamlessly overlap between them during the operation.

### A. Conventional Droop Control

In order to connect a number of VSCs in parallel and accomplish current sharing between them in distributed way, voltage control should not be stiff. So, the output voltage reference of every converter should follow VD characteristic defined with VR, which sets its stiffness measure. This concept stems from a practice of forming an electrical power system through speed-droop regulated governors of a number of parallel connected rotating synchronous generators [19]. Unlike the speed of rotating generators, the output voltage of converter is regulated here with respect to on-going condition of the grid, and is used as a system-wide control signal. This control concept utilizes two outer control loops which, when combined together, produce an output current reference. An output VR loop creates a voltage reference which is followed by the voltage loop:

$$v_{out}^* = v_{ref} - R_d i_o \qquad (1)$$

where $v_{out}^*$ is the voltage reference for voltage loop, $v_{ref}$ is the outer voltage reference, $i_o$ is the output current and $R_d$ is the VR.

Two specific cases of (1) can be distinguished. When VR takes the zero value, it corresponds to VSC. If it takes the infinite value, it corresponds to CSC. If the latter instance is considered, current reference will be generally set in such a
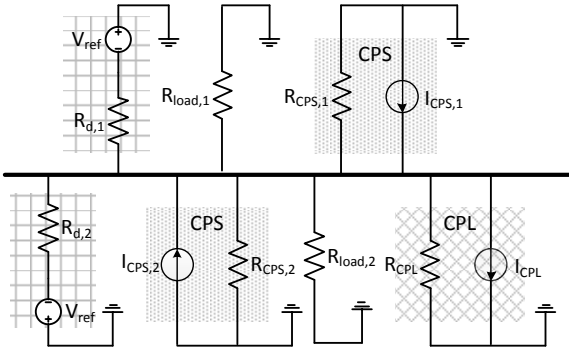
Fig. 2. Equivalent diagram of droop controlled dc microgrid.



Fig. 3. The i−P characteristic of a droop, MPPT and charge controlled unit.

way that the unit's extracted/injected power is constant. So, a constant power load (CPL) or constant power source (CPS) then stems from the CSC concept. These notations are used in the remainder of the paper, because they provide an accurate description of the behaviour of RESs in MPPT and batteries in regulated charging mode.

For instance, PV array and WTG are preferred to operate in MPPT mode and to inject maximum possible power whenever possible. However, as the conservation of common voltage amplitude should be a priority, it is mandatory for some of the other units to operate in VSC fashion. Batteries are good choice for this due to their bidirectional power-flow capability. So, any power difference between RES production and load consumption will be automatically handled by them. Consequently, the incidence of continuous excess of produced energy will eventually lead the batteries to the high SOC, a condition where regulated finish of charging, tackled in Section III-B, is strongly advisable. Throughout this time, the affected battery can not participate in voltage control and RESs should take over it in given situation. Therefore, both batteries and RESs can act as VSCs or CSCs/CPLs.

### B. Load Flow in Droop Controlled dc Microgrid

Static behaviour of a VD controlled source can be represented by a voltage source in series with VR [26], whereas a CPL can be linearised around its operating point, yielding a negative resistance in parallel with a current source [27]. It is important to emphasize that the representation of CPLs and CPSs is virtually identical in the load flow study, only the current and equivalent resistance signs are opposite. Equivalent diagram consisting of all aforementioned units is showed in Fig. 2. Here, CPSs represent units injecting constant power into a bus (i.e. PV and WTG in MPPT mode), while CPLs represent units that extract constant power from the bus (i.e. electronic loads or batteries during regulated charging).

Assuming that all of the VD controlled sources have the same outer reference voltage and line losses between units are negligible (which is reasonable for a small isolated system), dc MG load flow for a general number of sources and loads can be formulated by observing Fig. 2:

$$V_{DC} = \frac{\frac{v_{ref}}{R_d} - I_{CP}}{\frac{1}{R_d} + \frac{1}{R_{load}} + \frac{1}{R_{CP}}} \qquad (2)$$
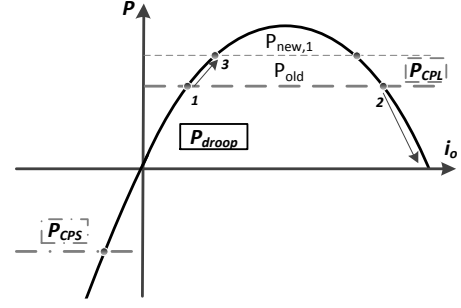
where $v_{ref}$ is the reference voltage. $R_d$ and $R_{load}$ are total system VR and resistive load, expressed as:

$$R_d = \frac{1}{\sum_{i=1}^{n} \frac{1}{R_{d,i}}} \qquad (3)$$

and

$$R_{load} = \frac{1}{\sum_{i=1}^{m} \frac{1}{R_{load,i}}} \qquad (4)$$

where $n$ is the number of sources presently operating in VD mode, and $m$ the number of resistive loads. It should be noted that if there is a non-negligible resistive loss on connection line between particular source and common busbar, it can be simply added to appropriate $R_{d,i}$. $I_{CP}$ and $R_{CP}$ are total current and resistance arising from CPLs and CPSs combination. As discussed in [27], linearised CPL can approximated by:

$$R_{CPL} = -\frac{V_{DC}^2}{P_{CPL}} \qquad (5)$$

$$I_{CPL} = 2\frac{P_{CPL}}{V_{DC}} \qquad (6)$$

where $P_{CPL}$ is the CPL power demand. If CPS is analysed instead, then reversed sign of $P_{CPS}$ will yield opposite signs in (5) and (6) as well. The combination of CPSs and CPLs may be represented with only one pair of current source and negative resistance, defined by dominant group of units. So, the equivalent $I_{CP}$ and $R_{CP}$ in (2) are computed as algebraic sums of corresponding terms. The inclusion of equivalent $I_{CP}$ and $R_{CP}$ in (2) results in a following expression:

$$aV_{DC}^2 + bV_{DC} + c = 0 \qquad (7)$$

with $a$, $b$ and $c$ being $\frac{1}{R_{load}} + \frac{1}{R_d}$, $-\frac{V_{ref}}{R_d}$ and $P_{CP}$ respectively. Solution of (7) for $V_{DC}$ gives an explicit solution for the common DC voltage:

$$V_{DC1,2} = \frac{\frac{v_{ref}}{R_d} \pm \sqrt{(\frac{v_{ref}}{R_d})^2 - 4P_{CP}(\frac{1}{R_d} + \frac{1}{R_{load}})}}{2(\frac{1}{R_d} + \frac{1}{R_{load}})}. \qquad (8)$$

There are two theoretical solutions of (8) which can also be seen in Fig. 3, where powers of equivalent CPL, CPS, and VD controlled source are expressed in dash, dash-dot and full line fashion respectively. Here, the $i - P$ plane has been

selected instead of $i-v$ for better visibility of the attraction of equilibrium points. To that extent, (1) was multiplied on both sides with the output current $i_o$ so as to obtain the power that VD controlled source injects into a common bus as a function of $i_o$:

$$P_{droop} = v_{ref}i_o - R_d i_o^2. \tag{9}$$

The equilibrium points are then the intersections of VD source line defined by (9) and CP line. Thus, for both voltage solutions, i.e. $V_{DC1}$ and $V_{DC2}$, there is an unique current that can be obtained through division of equivalent $P_{CP}$ with associated voltage.

In order to determine which one of these points is viable, there is no need for solving differential equations, but (8) is analysed as follows instead. As only one of the equivalent CPS or CPL can be more dominant, each case is analysed separately. So, if the CPSs are more dominant, $P_{CP}$ (labelled as $P_{CPS}$ in Fig. 3) has a negative sign and the square root expression in (8) becomes bigger than $\frac{V_{ref}}{R_d}$, making the second solution un-viable in this case. If the CPLs are more dominant, $P_{CP}$ (labelled as $P_{CPL}$ in Fig. 3) is positive and two viable solutions are possible. Two equilibriums that correspond to a certain $P_{CPL}$ are marked with *1* and *2* in Fig. 3. Now, if increase of CPL power from $P_{old}$ to $P_{new,1}$ at a certain moment is considered, VD controlled sources will start to reduce their output voltage according to (1) to meet new power expectation. Therefore, if starting point is *1*, the system will tend to go towards the new equilibrium point *3*. On the other hand, if starting point is *2*, it would go away from the equilibrium point *4*. Compatible response is obtained if CPL power is reduced. To conclude this discussion, it can be stated that only point *1* acts as an attractor. Thus, only $V_{DC1}$, the first solution of (8), is a stable equilibrium point.

Being able to establish this unique solution of the non-linear equation for any condition, one can use it for linear analysis in its infinitesimally small environment. This fact is especially suitable for cases where the system parameters are rapidly changing. So, it the voltage solution is included in (5), impact of droop control on the value of linearised CPL negative resistance becomes apparent as well. Both $V_{dc}$ and $R_{CPL}$ are plotted in Fig. 4 with constant resistive load of $4\Omega$ and changing the system equivalent VR. The representation of $I_{CPL}$ has been omitted as only the negative incremental resistance of $R_{CPL}$ tends to destabilize the system. Having a measure of $R_{CPL}$ for all operating points allows a linear analysis of the system that is inherently non-linear. This fact will be utilized in Section V, where small-signal stability is analysed for a complete range of changing VRs.

## III. MODELLING AND CONTROL OF ESS

In order to simulate and design the overall operation of a system properly, all the pieces of energy conversion process should be modelled. In particular, to study the behaviour of the system with special emphasis on battery management, it is important to have an accurate battery model. Provided the model is accurate, a significant gain in terms of time consumption and expense for designing the charging algorithms
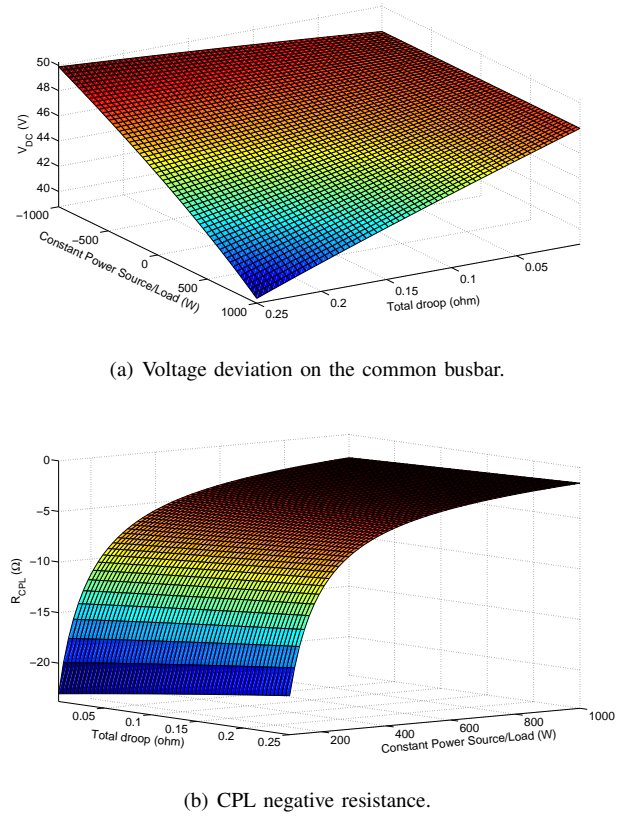


(a) Voltage deviation on the common busbar.



(b) CPL negative resistance.

Fig. 4. Voltage deviation for both CPS/CPL and negative CPL resistance with changing equivalent $R_d$.

and other specific control strategies can be achieved. Battery model and its control are shown in next two subsections.

### A. Battery model

A lot of research has been done in area of battery modelling, yielding several typical approaches; electrochemical, mathematical and electrical modelling. Electrical equivalent models generally best fit the overall application in circuit simulators, as they are constructed from classical network elements such as capacitors, resistors and voltage sources. It is agreed that voltage response of virtually all battery types can be approximated with voltage source in series with a number of RC elements, where each represents particular stage of relaxation during changing current conditions [28]. Model with a SOC dependent voltage source followed with one R and two RC elements has been developed for lithium-ion battery in [29] and is showed in Fig. 5. According to figure, battery terminal voltage follows next equation:

$$V_{terminal} = V_{OC} - I_{BAT}R(s) \tag{10}$$

where $V_{OC}$ is a SOC-dependant open-circuit voltage and $R(s)$ the equivalent battery resistance which can be expressed as:

$$R(s) = R_{si} + \frac{R_{tf}}{1 + sR_{tf}C_{tf}} + \frac{R_{ts}}{1 + sR_{ts}C_{ts}} \tag{11}$$

where $R_{si}$ is an instantaneous resistance, while $R_{tf}\&C_{tf}$ and $R_{ts}\&C_{ts}$ being RC pairs representing corresponding fast and slow relaxation terms.
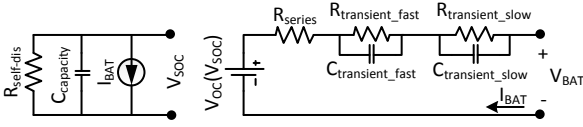
Fig. 5. Equivalent electrical model of the battery.

In this paper, identical modelling procedure was used to represent valve regulated lead-acid (VRLA) battery. Considered battery bank had a stated nominal 10 hour capacity of 420Ah and extraction procedure was done in similar fashion like in [30], but for a complete 24 VRLA battery cells connected in a series [31]. It resulted with following resulting parameters:

$$V_{OC}(SOC) = 0.035582 \cdot SOC + 47.698\,V \qquad (12)$$

$$R_{si} = 0.0401 \cdot e^{-0.0908 \cdot SOC} + 0.03655\,\Omega \qquad (13)$$

$$R_{tf} = 3.041 \cdot 10^{-10} \cdot e^{(0.1874 \cdot SOC)} + 0.03437\,\Omega \qquad (14)$$

$$R_{ts} = 0.101 \cdot e^{-0.02025 \cdot SOC} + 0.02188\,\Omega. \qquad (15)$$

The capacitances which determine the shape of battery voltage transient response did not show significant changes during the charge and discharge test procedure, and were modelled as constants with $C_{tf} = 1200\,F$ and $C_{ts} = 5000\,F$.

As demonstrated in [31], comparison of model presented here showed very good matching with experimental pulse charge/discharge tests and it is used for real-time battery simulations in this paper.

### B. Charge and Voltage Control

Appropriate charging is critically important to the life and performance of vented lead-acid and especially VRLA batteries [24]. While charging can be accomplished in various ways, limited-current followed by constant-voltage charging is the most effective and fastest method. For best results, the charging strategy should match the one proposed from battery manufacturer [32]. Two constant voltage charging values are often proposed over there; a float voltage and a boost voltage [33]. The float voltage is used as a first voltage value to fully charge the battery and is usually between 2.30 V to 2.40 V per cell for VRLA batteries. The boost voltage is usually higher, ranging from 2.40 V to 2.50 V per cell, and is needed in applications where battery string experiences frequent deep discharge conditions. Its purpose is to prevent the electrolyte stratification in the battery by releasing the gas. For long series strings of battery cells with slight differences in internal impedances, it is also useful to provide periodical capacity equalization. Therefore, most of the VRLA battery chargers are able to operate on both values. As deep discharge cycles should be expected in autonomous dc MG applications, both boost and float voltages are used for charging in this paper.

Complete battery control diagram is presented in Fig. 6, where the circuit from the upper part performs internal charge regulation, while the bottom part does the common VD control. Current loops are the same for both circuits.
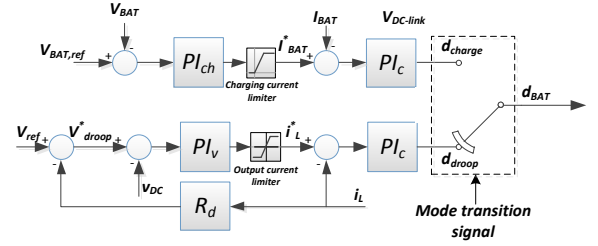


Fig. 6. Block diagram representation of outer and inner control loops for batteries.

These two unit-level modes of operation can be interactively interchanged through the switch controlled by the supervisory control, which is marked with red colour. Smooth transition for unit-level mode transitions is achieved by means of enforcing the initial conditions of inactive PI current controller to the value of the output of active one. Current limiter for the output inductor current, also indicated with red colour, is used to disable current flow in particular conditions, and is controlled from supervisory control as well.

### C. Adaptive droop calculation

Possible expansion of the MG in terms of increase of load should be accompanied by an expansion of production and storage capacity. As battery cells that were already connected are usually set up within a specialized metal construction inside of a container and their interfacing converter is generally selected for specified input voltage, it is not practical to add new cells to existing arrangement. Connection of new battery string is therefore mostly the best option.

However, as the new battery string will not necessary be the same as the old one, this kind of expansion brings in certain challenges. In isolated system, batteries will mostly operate in the VD mode and their current flow will then depend on VRs. It is therefore not viable to use the same value for two batteries with different capacities or initial SOCs, because their SOC difference will not eventually fade away in that case. As good life-cycle is expected for batteries with as small depth of discharge as possible [24], it is felt by the authors that the best compromise is to try and keep the equal SOC of all the batteries within the system. In order to do this in general system consisting of arbitrary number of batteries, a battery with the highest SOC should be always discharged at the most rapid rate, while a battery with the lowest one with the slowest rate. The contrary consideration must be taken into an account while charging.

To accomplish this goal, one possibility is a SOC dependant adaptive change of the VRs. The value of $R_{d,i}$ should correspond to the current SOC and capacity of the battery $i$. Higher $R_{d,i}$ will cause lower charge/discharge rate and vice-versa. Therefore, when batteries are charging, higher $R_{d,i}$ should be given to a battery with higher SOC. On the other hand, when discharging, higher $R_{d,i}$ should be given to battery with lower SOC. One option to enforce VRs to follow this law is to adapt them according to symmetric SOC dependant functions for charge and discharge conditions. Moreover, as the rate of change of SOC is inversely proportional to battery capacity , $C_{BAT}$ should also be taken into an account as a scaling coefficient. SOC of a battery $i$ is computed as follows
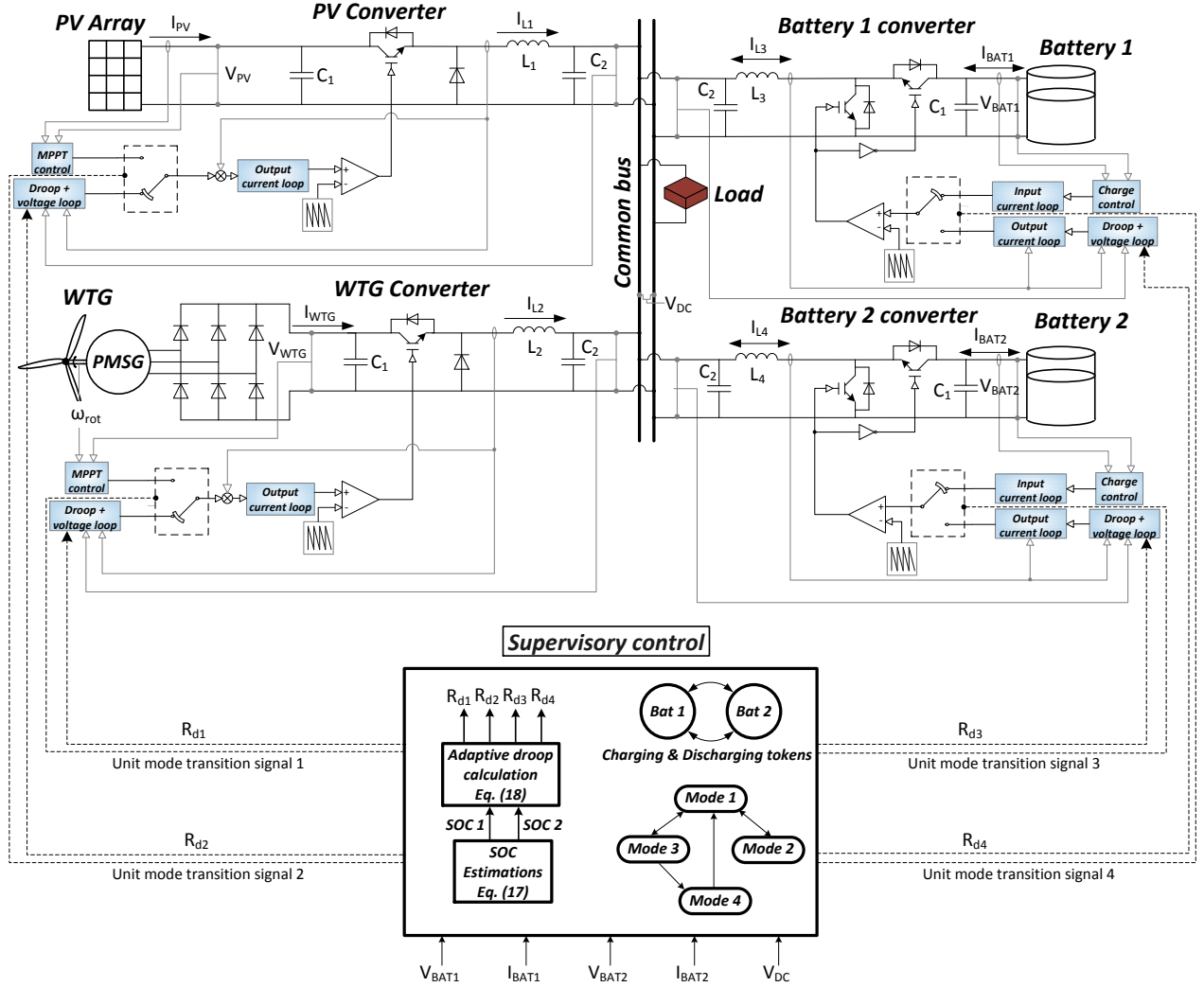
Fig. 7.   Complete configuration of dc MG with primary and supervisory control schematic.

$$SOC_i(t) = SOC_i(0) - \int_0^t \eta_i \frac{I_{BAT,i}(\tau)}{C_{BAT,i}}(\tau)\,d\tau \qquad (16)$$

where $SOC_i(0)$ is inital SOC, $\eta_i$ is charging/discharging efficiency, $I_{BAT,i}$ is battery current and $C_{BAT,i}$ is the nominal capacity. As a solution to above considerations, a symmetric function for computing charge and discharge VRs, taking into an account batteries' SOCs and its rate of change, has been proposed as follows:

$$\begin{cases} R_{d,i,charge} = \frac{C_{BAT,i}}{C_{max}}\alpha \cdot exp(\beta \cdot SOC) \\ R_{d,i,discharge} = \frac{C_{BAT,i}}{C_{max}}\alpha \cdot exp(\beta \cdot (100 - SOC)) \end{cases}$$
$$(17)$$

where $C_{max}$ is the capacity of the battery with highest nominal capacity in the system. The reason of using exponential rather than linear function is to enforce the faster approaching of batteries SOCs.

## IV. SUPERVISORY ENERGY MANAGEMENT SYSTEM

Fig. 7 shows a complete control schematic of analysed MG. Proposed supervisory control monitors the variables from local controllers and performs its three main functionalities; Determination of system-level operating modes, passing of

charging/discharging tokens and calculation of VRs based upon SOC estimation. As there are two battery banks connected to the main bus, supervisory control was designed to regulate their charging and discharging in coordinated manner as to preserve their cycle life, but not compromising the common voltage control. To do so, several prescriptions were put on:

- During the normal operation, the batteries' SOCs are enforced to asymptotically approach each other through an adaptive VRs calculation.
- Battery with higher initial SOC is first to be fully charged.
- If there is enough production in the system, batteries are kept fully charged.
- Once both batteries are charged, the one that was first charged is the one to start discharging first as well.
- If one battery is charged, it will start discharging once the SOC of the other falls below 90%.

If these prescriptions are respected, batteries will be fully charged in a round-robin manner. Also, the battery that is fully charged will be kept at that state as long as possible. Four system-level operating modes arise from this considerations. Modes and equivalent diagrams that correspond to every operating mode are depicted in Fig. 8 and Fig. 9 respectively, and are clarified as follows
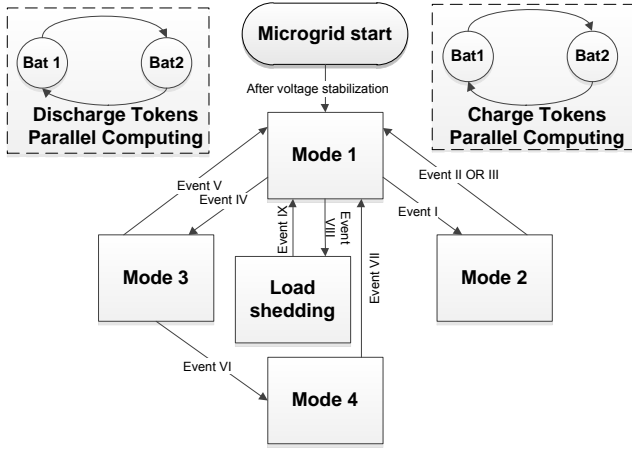
Fig. 8. Even-driven flowchart of the system.

## A. Mode I−Normal operating mode

MPPT algorithms for RESs and VD control for batteries are active. Adaptive calculation of VRs for batteries is activated as well, and depending on RESs production and load requirements, batteries are charged or discharged. SOC calculation is based on coulomb-counting method (16), but advanced SOC estimators can also be used [34]. Supervisory control monitors SOCs of both batteries in this mode and gives a charging token to the battery with higher SOC. This functionality is important because battery with charging token will be the first one to start with regulated charging. However, if one of the batteries was initially full, it is held in a floating mode, which means that it draws as much current as needed to keep its voltage at $V_{float}$. Its discharge is enabled once the SOC of the battery in VD mode falls below 90%.

A prolonged disbalance between available and consumed power will lead batteries to a boundary levels of SOC; If high margin is reached, regulated charging of battery with the charging token will be initiated, while load-shedding is the only option if low margin is reached. Load shedding scheme is out of the scope of this paper, but common voltage value can be used as a detector for its execution. Event VII and Event IX denote entrance and exit from common-voltage based load-shedding.

## B. Mode II−First Charging Mode

For initiation of regulated charging, battery voltages are used as a trigger rather than SOC itself, as they are directly measurable and less sensitive to errors that are generally present in SOC estimators. So, when voltage of battery with the token reaches $V_{trig}$ value (Event I), supervisory control transfers the RESs to VD control at first and after 0.5s acts on battery switch and moves it into the regulated charging mode. The 0.5s delay was used to reduce the impact of the switching transient in the system. To disable discharging the other battery, its output current limiter is activated. Once the charging algorithm is executed (Event II), battery is fully charged and automatically receives the discharging token. Supervisory control resets its SOC to exactly 100% and passes the charging token to the other battery. After this actions, system returns to Mode I.



(a) Mode 1
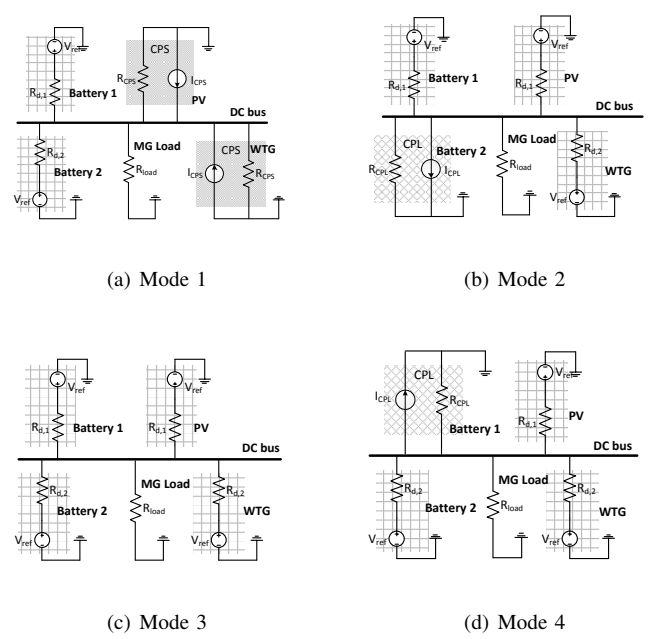
(b) Mode 2

(c) Mode 3

(d) Mode 4

Fig. 9. Equivalent circuits of the system under different modes.

It might happen that a sudden reduction of available power from RESs occurs during the process of regulated charging to an extent where there is not enough of it to supply the load as well (Event III). Then, the voltage on the common bus will start to decrease. Therefore, a low voltage threshold, $V_{low}$, is used to detect this condition and to take the system back to Mode I.

## C. Mode III−Second Charging Mode

Transition to Mode III can be enabled exclusively from Mode I. It will happen if one battery is full and voltage of the other one reaches $V_{trig}$ value (Event IV). Then again, VD is activated for RESs and after 0.5s this battery enters the regulated charging mode. If charging algorithm is completed successfully (Event VI), SOC of newly charged battery is set to exactly 100% and the system is moved to Mode IV.

On the other hand, if execution of the charging algorithm is disrupted by sudden disbalance of RESs production and load (Event V), again $V_{low}$ is used to detect it and transit the system to Mode I.

## D. Mode IV−Full SOC Mode

Mode IV is active when both batteries are completely full and operate in floating mode, while RESs are in the VD mode. Again, $V_{low}$ is used to detect if load consumption has become higher than maximum RESs production. Then, supervisory control activates VD control of the battery with discharging token and its discharging is started to restore the common voltage. As this mode can be enabled exclusively from Mode III, it necessarily must have passed through Mode II. In that mode, battery that was first fully charged received the discharging token and so it is now the first to start the discharge. Therefore, once the common voltage reaches $V_{low}$ (Event VII), Mode I is activated again.
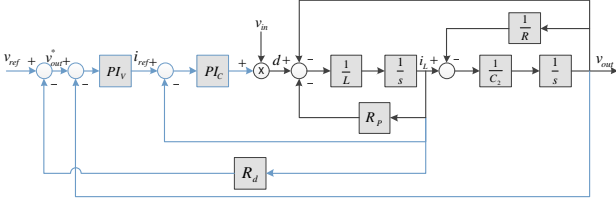
Fig. 10. Block diagram representation of a bidirectional converter with the droop-control technique implemented.

Following the execution of Mode IV, a complete cycle through all modes is made. Battery that was first charged now has lower SOC than the other one. Next charging token is automatically taken by the latter, making the charge completion for batteries taking place in a round-robin manner. It is also made sure that always two sources operate with the VD control so as to regulate the common voltage at every time.

In next section, state of the system that presents a worst-case condition in terms of stability is pointed up and a small-signal model is built to prove the stability in the latter.

## V. SMALL-SIGNAL ANALYSIS

Depending on the operating mode, two possible control strategies can be active within one source, where every one of them brings in particular features in terms of stability. So, RESs can be VD regulated or controlled with MPPT algorithms (CPLs), while batteries can be charged in regulated manner (CPSs) or be VD regulated as well.

Referring to (5) and (6), a perfect CPL can be modelled as a negative incremental resistance in parallel with positive current source. On the other hand, model of perfect CPS contains positive incremental resistance and negative current source. The constant current sources have no impact on stability, but the equivalent resistances influence the damping of the system; negative resistance decreases, while the positive one increases it [35]. There are several factors that affect the level of agreement of practical CPSs/CPLs and the perfect ones, namely the efficiency of associated converter and its closed loop gain and bandwidth. So, the negative impact of practical CPL on system damping will be less significant than that of the perfect one as well as positive impact of practical CPS [36]. Thus, if stability is guaranteed for perfect CPL, system would also be stable with practical one.

If above considerations are taken into an account, it can be concluded that instability will most likely be induced during the boost voltage charging in modes II and III as charged batteries bring in the minimum negative resistance in that stage. If the system load is light and only one RES is available during that time as well, this can be considered as a worst-case condition. So, if closed-loop stability can be ensured here, system should be stable in all operating modes.

Block diagram of VD control applied to a synchronous buck converter is shown in Fig. 10. Characteristic equation arising from the diagram can be expressed as a fourth order function:

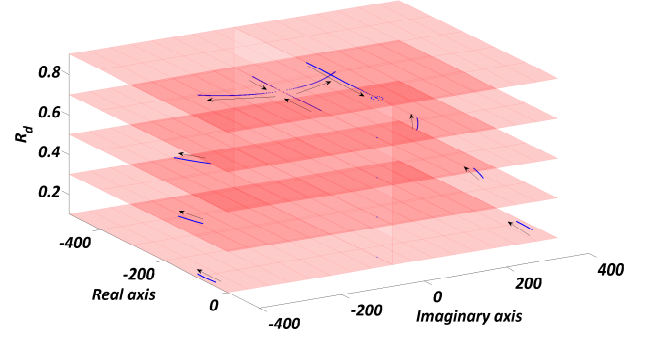$$s^4 + \alpha s^3 + \beta s^2 + \gamma s + \delta = 0 \qquad (18)$$

where



Fig. 11. Family of root locus for changing the CPL of the system from P=600W to P=0.

$$\alpha = \frac{R_d P_c P_v V_{in} + P_c V_{in} + R_p}{L} + \frac{1}{C R} \qquad (19)$$

$$\beta = \frac{V_{in} (I_c + R_d I_c P_v + R_d I_v P_c)}{L} + \frac{R + R_p + P_c V_{in} + R_d P_c P_v V_{in} + P_c P_v R V_{in}}{C L R} \qquad (20)$$

$$\gamma = \frac{R_d I_c I_v V_{in}}{L} + \frac{I_c P_v V_{in}}{C L} + \frac{I_v P_c V_{in}}{C L} + \frac{I_c V_{in}}{C L R} + \frac{R_d I_c P_v V_{in}}{C L R} + \frac{R_d I_v P_c V_{in}}{C L R} \qquad (21)$$

$$\delta = \frac{I_c I_v V_{in}}{C L} + \frac{R_d I_c I_v V_{in}}{C L R} \qquad (22)$$

with $R$ being the total equivalent resistance seen by the system, $L$, $C$ and $R_p$ being the converter output capacitance, inductance and switch and inductor losses respectively. $P_v$, $I_v$ and $P_c$ are the control parameters and $V_{in}$ is the input voltage. If charging algorithm in Subsection III-B is reconsidered, maximum power that a battery extracts from the system during its charging can be approximated by:

$$P_{BAT,max} = V_{boost} \cdot I_{ch} \qquad (23)$$

where $I_{ch}$ is a current limitation in charging mode. As supervisory control makes sure that only one battery is in charging mode at the time, maximum resistance arising from this occurrence can be expressed similar as (5):

$$R_{ch,min} = -\frac{V_{DC}^2}{P_{BAT,max}} \qquad (24)$$

where $V_{DC}$ is the viable solution of (8). To obtain a worst-case loading resistance of the system, $R_{ch,min}$ should be hooked up with other CPLs and resistive loads that correspond to worst-case condition in terms of stability:

$$R = R_{ch,min} || R_{CPL,min} || R_{LOAD,max} \qquad (25)$$

where $R_{CPL,min}$ is a maximum expected resistance from other CPLs computed from (5) and $R_{LOAD,max}$ is a maximum expected resistance from resistive loads.

TABLE I
EXPERIMENTAL SETUP PARAMETERS

| Parameter | Symbol | Values |
|---|---|---|
| Converters | | |
| DC power supply | $V_{in}$ | 100 V |
| Switching frequency | $f_{sw}$ | 10 kHz |
| Input capacitance | $C_1$ | 2.2e-3 F |
| Total output capacitance | $C_2$ | 4×2.2e-3 F |
| Converter inductances | $L$ | 1.8e-3 H |
| Inductor+switch loss resistance | $R_p$ | 0.1 Ω |
| Primary control | | |
| Reference voltage | $V_{ref}$ | 48 V |
| Proportional current term | $P_c$ | 2 |
| Integral current term | $I_c$ | 97 |
| Proportional voltage term | $P_v$ | 0.5 |
| Integral voltage term | $I_v$ | 994 |
| Inductor current limits | $I_{lim}$ | ±7 A |
| Charging algorithm | | |
| Proportional voltage term | $P_{ch}$ | 7.5 |
| Integral voltage term | $I_{ch}$ | 994 |
| Charge triggering voltage | $V_{trig}$ | 54 V |
| Boost voltage | $V_{boost}$ | 58.2 V |
| Float voltage | $V_{float}$ | 55.2 V |
| Charging current limit | $I_{ch}$ | 6 A |
| Busbar voltage monitoring | | |
| Mode switch trigger | $V_{low}$ | 45 V |

As $R_d$ is adapted with battery capacities and SOCs accord-
ing to (17), a family of root locus for different $R_d$ has been
plotted in Fig. 11 for changing the power of equivalent CPL
in the system from 0W to 600W. $R_{LOAD,max}$ was set to be
15Ω, as it can be considered as a relatively light. Including
this values into equations (5) and (8), $R_{CPL}$ was computed
and combined again with $R_{LOAD,max}$ to get an equivalent $R$.
Rest of the parameters needed to evaluate 18 are provided in
Table I.

As shown in Fig. 11, $R_d$ values between 0.1 and 0.9 showed
good small-signal behaviour. Arrows denote the propagation
of dominant poles with decrease of equivalent CPL. Chosen
values of $R_d$ do not bring big voltage deviations to the system,
so $\alpha$ and $\beta$ used for adaptive VR calculations in (17) have been
chosen to be 0.1 and 0.023 respectively.

## VI. EXPERIMENTAL RESULTS

In order to validate the proposed hierarchical control strat-
egy, four unit system shown in Fig. 7 was built in a laboratory.
Batteries have been modelled in Matlab/Simulink according
to model presented in Sec. III-A. To perform the tests in
reasonable time, nominal capacity of both batteries was set
up to 0.2 Ah. Hence, to keep the model scaled, the capac-
itances of relaxation terms were also appropriately adapted.
Matlab/Simulink has also been used for implementation of
primary control, where PV array and WTG were emulated as
CPSs in MPPT mode, and the same as batteries in VD mode,
but with limitation of maximum power. Maximal power of PV
array was set to 350W, while the power of WTG was set to
200W. Supervisory control was developed in Matlab/Stateflow.
The final code was compiled into a dSPACE ds1103 platform
for real time control of the experimental setup. Omission of
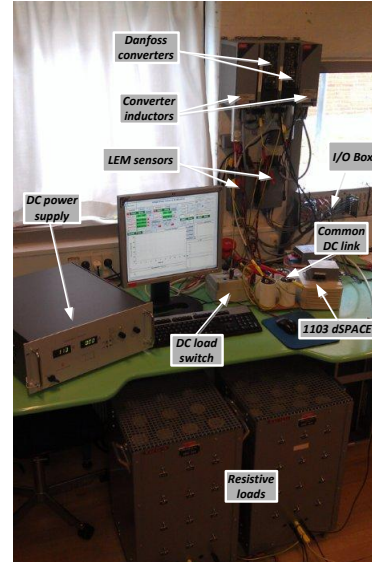the detailed models of PV and WTG and their dedicated
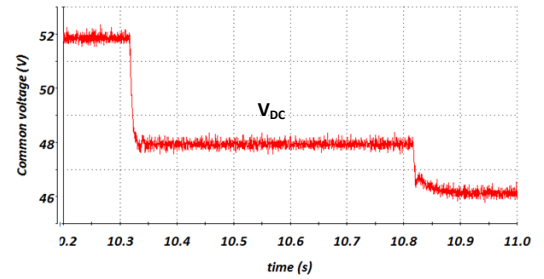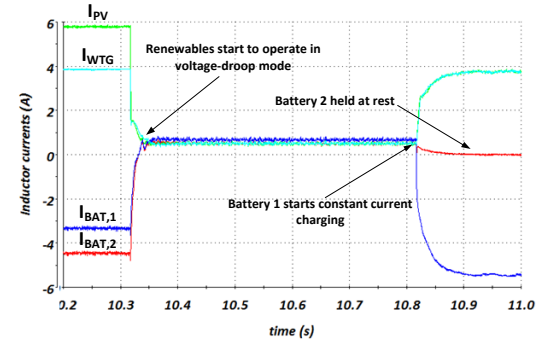


Fig. 12. Experimental setup.



(a) Common DC voltage.



(b) Inductor currents.

Fig. 13. Results for transition from Mode I to Mode II.

MPPT algorithms was done due to the memory limit of
the dSPACE platform. Nevertheless, as the bandwidth of the
primary control level is normally much higher than those of
MPPT algorithms, the impact of this simplifications virtually
does have no impact on the MG side of the system.

Setup, showed in Fig. 12 consists of four synchronous
buck converters supplied by Delta-Elektronika SM 600-10
dc power supply. Two parallel variable resistors of minimum
6.7Ω were used to emulate the system load. A list of system
parameters significant for this study is presented in Table I.
Experiments have been carried out for transient performance
during transitions between system-level operating modes.
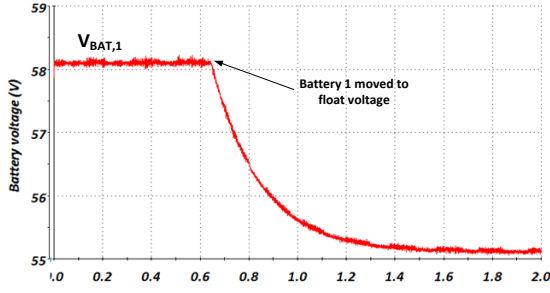
(a) Battery #1 voltage.
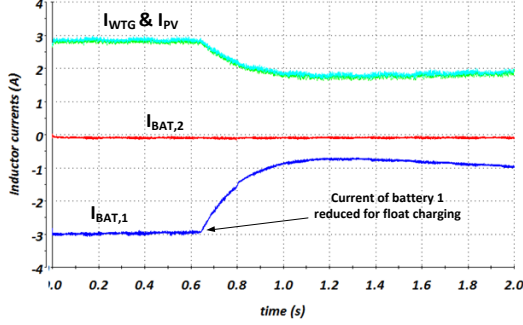


(b) Inductor currents.

Fig. 14. Transition from boost fo float charging in Mode II.



(a) Common DC voltage.



(b) Inductor currents.

Fig. 15. Results for transition from Mode II back to Mode I after completing the charging algorithm for battery #1.

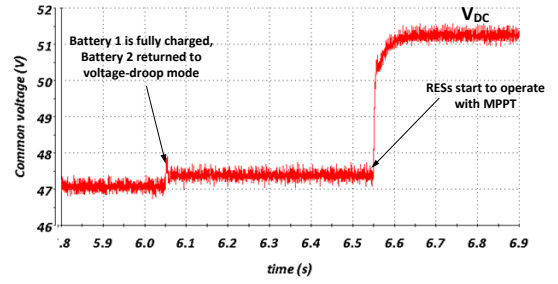## A. Testing the Transition From Mode I to Mode II

During Mode I, an adaptive droop calculation of VRs presented in Section III-C is activated, and the SOCs of the batteries will not cross each other. So, the charging token will be occupied by the battery with higher initial SOC, which is battery#1 in this case. MPPT algorithms for PV array and WTG are on and any power difference between power demanded by loads and produced one is handled by batteries.

Here, there is a surplus of available production and the batteries are charging. When the voltage of battery#1 reaches $V_{trig}$, system is transferred to Mode II. Insight into this transient is given in Fig. 13. In Mode II, RESs start to operate with VD control using the same VR as battery#2. After 0.5s, battery#1 starts regulated charging and battery#2 is put into a current-limited mode.
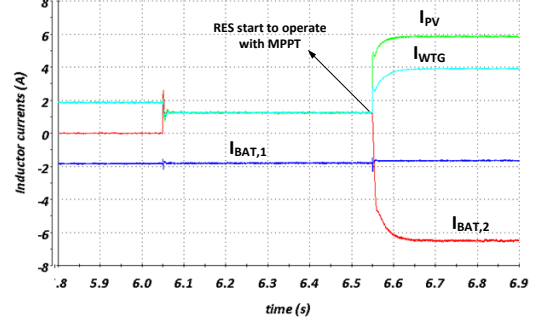
With initiation of regulated charging, charging algorithm described in III-B is performed. This means that at first, the battery is charged with limited current until $V_{boost}$ is reached. Then, after specified amount of time, this voltage is reduced to $V_{float}$ This transient is shown in Fig. 14.

## B. Testing the Return From Mode II to Mode I

Production from RESs is enough to supply the consumption and needs of regulated battery charging throughout the execution of the charging algorithm and elapsed time for constant voltage charging triggers the return of the system from Mode II to Mode I. Battery#1 is now fully charged and the discharging token is given to it. Battery#2 returns from current-limited mode to VD control instantly and after 0.5s RES start to operate with MPPT again. This event is shown in Fig. 15.

## C. Testing the Transition From Mode I to Mode III

Mode III is activated if one of the batteries is full and the other one reaches the $V_{trig}$ value. In this case, battery#2 starts its regulated charging with battery#1 being fully charged, but equivalent results would be obtained if the situation is inverse. So, at first, RES are switched from MPPT to VD control using the same VR as battery#2. After 0.5s battery#2 starts with constant current charging. This event is shown in Fig. 16.

As in Mode II, battery reaches the $V_{boost}$, which is eventually lowered to $V_{float}$ value.

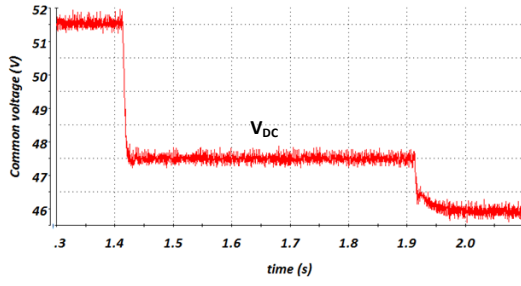## D. Transition From Mode III to Mode IV

If RESs were able to maintain the common voltage throughout the charging of the battery#2, system is moved to Mode IV after successful execution of the algorithm. This means that both batteries are kept at $V_{float}$ voltage value and RES operate in VD mode. This mode will now remain active as long as there is enough RESs power available.

## E. Testing the Return From Mode IV to Mode I

Both batteries are kept full in Mode IV and RESs regulate the voltage. However, with big increase of load at some point, RESs production is not enough to supply the it any more. Now, the common voltage starts to decrease. Triggering value of $V_{low}$ is used to detect this condition and once it happens, battery#1, which holds the discharging token will exit the floating mode and start with VD control. This event is shown in Fig. 17.

## F. Testing the Exit from Current Limit in Mode I

Load has been kept high for a prolonged time and SOC of battery #1 falls below 90%. This triggers the start of
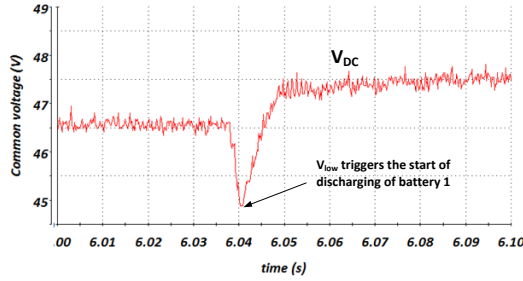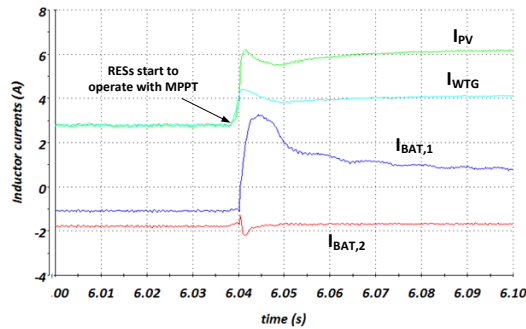
(a) Common DC voltage.
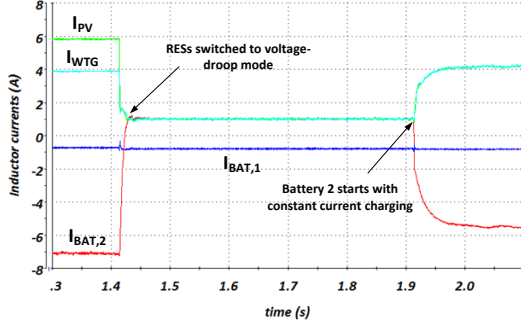


(b) Inductor currents.

Fig. 16. Results for transition from Mode I to Mode III



(a) Inductor currents.

Fig. 18. Start of discharging battery #2

munication power systems was developed. Environment suitable for efficient management of batteries was created by combining dual-role primary control with higher level supervisory control which can be implemented through low-bandwidth communication interface. Avoidance of considerable voltage deviation and ability of coordinated charging of multiple batteries are the main advantages achieved from proposed control when compared with traditional methods. Also, an adaptive droop calculation method was proposed and incorporated within the supervisory control to assure the asymptotic SOC approaching for arbitrary number of batteries. As VRs impact the stability of the system, small-signal model was developed and stability was assessed taking into account unit-level operating modes. Experimental tests for changing mode conditions have been carried out to validate the proposed control approach, showing smooth transitions between system-level modes.

discharging of battery#2 as well. With this event, which is shown in Fig. 18, system finishes a complete cycle and returns back to initial point. Battery#1 now has a lower SOC than battery#2, so the next charging token is given to it. This way, regulated charging for multiple batteries within the system is performed in a round-robin manner.
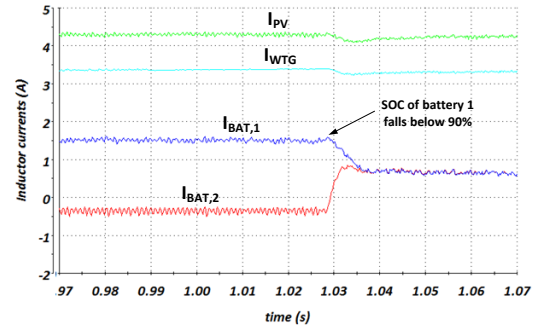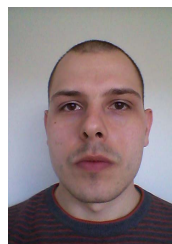


(a) Common DC voltage.



(b) Inductor currents.

Fig. 17. Results for transition from Mode IV back to Mode I

## VII. CONCLUSION

In this paper, a control strategy for autonomous dc MG applicable to low voltage applications such as remote telecom-

## REFERENCES

[1] F. Blaabjerg, Z. Chen, and S. Kjaer, "Power Electronics as Efficient Interface in Dispersed Power Generation Systems," *IEEE Transactions on Power Electronics*, vol. 19, pp. 1184–1194, Sept. 2004.

[2] R. Lasseter, "MicroGrids," in *2002 IEEE Power Engineering Society Winter Meeting. Conference Proceedings (Cat. No.02CH37309)*, vol. 1, pp. 305–308, IEEE.

[3] N. Pogaku, M. Prodanovic, and T. C. Green, "Modeling, Analysis and Testing of Autonomous Operation of an Inverter-Based Microgrid," *IEEE Transactions on Power Electronics*, vol. 22, pp. 613–625, Mar. 2007.

[4] F. Katiraei, M. Iravani, and P. Lehn, "Micro-Grid Autonomous Operation During and Subsequent to Islanding Process," *IEEE Transactions on Power Delivery*, vol. 20, pp. 248–257, Jan. 2005.

[5] J. Guerrero, J. Vasquez, J. Matas, M. Castilla, and L. de Vicuna, "Control Strategy for Flexible Microgrid Based on Parallel Line-Interactive UPS Systems," *IEEE Transactions on Industrial Electronics*, vol. 56, pp. 726–736, Mar. 2009.

[6] A. Dimeas and N. Hatziargyriou, "Operation of a Multiagent System for Microgrid Control," *IEEE Transactions on Power Systems*, vol. 20, pp. 1447–1455, Aug. 2005.

[7] Y. W. Li and C.-N. Kao, "An Accurate Power Control Strategy for Power-Electronics-Interfaced Distributed Generation Units Operating in a Low-Voltage Multibus Microgrid," *IEEE Transactions on Power Electronics*, vol. 24, pp. 2977–2988, Dec. 2009.

[8] D. Salomonsson, L. Soder, and A. Sannino, "Protection of Low-Voltage DC Microgrids," *IEEE Transactions on Power Delivery*, vol. 24, pp. 1045–1053, July 2009.

[9] H. Kakigano, Y. Miura, and T. Ise, "Low-Voltage Bipolar-Type DC Microgrid for Super High Quality Distribution," *IEEE Transactions on Power Electronics*, vol. 25, pp. 3066–3075, Dec. 2010.

[10] J. Schonberger, R. Duke, and S. Round, "DC-Bus Signaling: A Distributed Control Strategy for a Hybrid Renewable Nanogrid," *IEEE Transactions on Industrial Electronics*, vol. 53, pp. 1453–1460, Oct. 2006.

[11] K. Sun, L. Zhang, Y. Xing, and J. M. Guerrero, "A Distributed Control Strategy Based on DC Bus Signaling for Modular Photovoltaic Generation Systems With Battery Energy Storage," *IEEE Transactions on Power Electronics*, vol. 26, pp. 3032–3045, Oct. 2011.

[12] R. S. Balog and P. T. Krein, "Bus Selection in Multibus DC Microgrids," *IEEE Transactions on Power Electronics*, vol. 26, pp. 860–867, Mar. 2011.

[13] D. Boroyevich, I. Cvetkovic, D. Dong, R. Burgos, F. Wang, and F. Lee, "Future electronic power distribution systems a contemplative view," in *2010 12th International Conference on Optimization of Electrical and Electronic Equipment*, pp. 1369–1380, IEEE, May 2010.

[14] K. Schneider, C.-C. Liu, and B. Howe, "Topology Error Identification for the NEPTUNE Power System," *IEEE Transactions on Power Systems*, vol. 20, pp. 1224–1232, Aug. 2005.

[15] J. Ciezki and R. Ashton, "Selection and stability issues associated with a navy shipboard DC zonal electric distribution system," *IEEE Transactions on Power Delivery*, vol. 15, pp. 665–669, Apr. 2000.

[16] B. Cho and F. Lee, "Modeling and analysis of spacecraft power systems," *IEEE Transactions on Power Electronics*, vol. 3, no. 1, pp. 44–54, 1988.

[17] F. Valenciaga and P. Puleston, "Supervisor Control for a Stand-Alone Hybrid Generation System Using Wind and Photovoltaic Energy," *IEEE Transactions on Energy Conversion*, vol. 20, pp. 398–405, June 2005.

[18] J. M. Guerrero, L. Hang, and J. Uceda, "Control of Distributed Uninterruptible Power Supply Systems," *IEEE Transactions on Industrial Electronics*, vol. 55, pp. 2845–2859, Aug. 2008.

[19] P. Kundur and N. J. Balu, *Power System Stability and Control*. McGraw-Hill, 1998.

[20] J. M. Guerrero, J. C. Vasquez, J. Matas, L. G. de Vicuna, and M. Castilla, "Hierarchical Control of Droop-Controlled AC and DC MicrogridsA General Approach Toward Standardization," *IEEE Transactions on Industrial Electronics*, vol. 58, pp. 158–172, Jan. 2011.

[21] P. Karlsson and J. Svensson, "DC bus voltage control for a distributed power system," *IEEE Transactions on Power Electronics*, vol. 18, pp. 1405–1412, Nov. 2003.

[22] D. Sera, R. Teodorescu, J. Hantschel, and M. Knoll, "Optimized Maximum Power Point Tracker for Fast-Changing Environmental Conditions," *IEEE Transactions on Industrial Electronics*, vol. 55, pp. 2629–2637, July 2008.

[23] A. Knight and G. Peters, "Simple Wind Energy Controller for an Expanded Operating Range," *IEEE Transactions on Energy Conversion*, vol. 20, pp. 459–466, June 2005.

[24] D. Linden and T. B. Reddy, *Handbook of Batteries*. McGraw-Hill, 2002.

[25] B. Borowy and Z. Salameh, "Methodology for optimally sizing the combination of a battery bank and pv array in a wind/pv hybrid system," *Energy Conversion, IEEE Transactions on*, vol. 11, pp. 367 –375, jun 1996.

[26] B. Johnson, R. Lasseter, F. Alvarado, and R. Adapa, "Expandable multiterminal DC systems based on voltage droop," *IEEE Transactions on Power Delivery*, vol. 8, no. 4, pp. 1926–1932, 1993.

[27] A. Rahimi and A. Emadi, "Active Damping in DC/DC Power Electronic Converters: A Novel Method to Overcome the Problems of Constant Power Loads," *IEEE Transactions on Industrial Electronics*, vol. 56, pp. 1428–1439, May 2009.

[28] S. Barsali and M. Ceraolo, "Dynamical models of lead-acid batteries: implementation issues," *IEEE Transactions on Energy Conversion*, vol. 17, pp. 16–23, Mar. 2002.

[29] M. Chen and G. Rincon-Mora, "Accurate Electrical Battery Model Capable of Predicting Runtime and IV Performance," *IEEE Transactions on Energy Conversion*, vol. 21, pp. 504–511, June 2006.

[30] S. Abu-Sharkh and D. Doerffel, "Rapid test and non-linear model characterisation of solid-state lithium-ion batteries," *Journal of Power Sources*, vol. 130, pp. 266–274, May 2004.

[31] T. Dragicevic, T. Capuder, M. Jelavic, and D. Skrlec, "Modelling and Simulation of Isolated DC Microgrids Supplied by Renewable Energy Resources, volume = 1," in *2011, Conference on Sustainable Development of Energy, Water and Environment Systems*.

[32] *IEEE Std 1561, IEEE Guide for Optimizing the Performance and Life of Lead-Acid Batteries in Remote Hybrid Power Systems*.

[33] T. Support, "Installation, Commissioning and Operation Handbook for Gel-VRLA-Batteries." http://www.sonnenschein.org/PDF%20files/ GelHandbookPart2.pdf, 2003. [Online; accessed 01-September-2012].

[34] G. Plett, "Extended kalman filtering for battery management systems of lipb-based hev battery packs: Part 3. state and parameter estimation," *Journal of Power Sources*, vol. 134, no. 2, pp. 277–292, 2004.

[35] A. Rahimi, G. Williamson, and A. Emadi, "Loop-cancellation technique: A novel nonlinear feedback to overcome the destabilizing effect of constant-power loads," *Vehicular Technology, IEEE Transactions on*, vol. 59, pp. 650 –661, feb. 2010.

[36] A. Rahimi and A. Emadi, "An analytical investigation of dc/dc power electronic converters with constant power loads in vehicular power systems," *Vehicular Technology, IEEE Transactions on*, vol. 58, pp. 2689 –2702, july 2009.

**Tomislav Dragičević** (S'09) received the M.E.E. and the Ph.D. degree from the Faculty of Electrical Engineering, Zagreb, Croatia, in 2009 and 2013, respectively. Since 2010, he has been actively cooperating in an industrial project related with design of electrical power supply for remote telecommunication stations. He is currently a full-time Post-Doc at Aalborg University in Denmark. His fields of interest include modeling, control and energy management of direct current distributed power systems based on renewable energy sources and energy storage technologies.

**Josep M. Guerrero** (S'01-M'04-SM'08) received the B.S. degree in telecommunications engineering, the M.S. degree in electronics engineering, and the Ph.D. degree in power electronics from the Technical University of Catalonia, Barcelona, in 1997, 2000 and 2003, respectively. He was an Associate Professor with the Department of Automatic Control Systems and Computer Engineering, Technical University of Catalonia, teaching courses on digital signal processing, field-programmable gate arrays, microprocessors, and control of renewable energy. In 2004, he was responsible for the Renewable Energy Laboratory, Escola Industrial de Barcelona. Since 2011, he has been a Full Professor with the Department of Energy Technology, Aalborg University, Aalborg East, Denmark, where he is responsible for the microgrid research program. From 2012 he is also a guest Professor at the Chinese Academy of Science and the Nanjing University of Aeronautics and Astronautics. His research interests are oriented to different microgrid aspects, including power electronics, distributed energy-storage systems, hierarchical and cooperative control, energy management systems, and optimization of microgrids and islanded minigrids. Prof. Guerrero is an Associate Editor for the IEEE Transactions on Power Electronics, the IEEE Transactions on Industrial Electronics, and the IEEE Industrial Electronics Magazine. He was the chair of the Renewable Energy Systems Technical Committee of the IEEE Industrial Electronics Society.

**Juan C. Vasquez** (M'12) received the B.S. degree in Electronics Engineering from Autonoma University of Manizales, Colombia in 2004 where he has been teaching courses on digital circuits, servo systems and flexible manufacturing systems. In 2009, He received his Ph.D. degree from the Technical University of Catalonia, Barcelona, Spain in 2009 at the Department of Automatic Control Systems and Computer Engineering, from Technical University of Catalonia, Barcelona (Spain), where he worked as Post-doc Assistant and also teaching courses based on renewable energy systems. Currently, he is an Assistant Professor at Aalborg University in Denmark. His research interests include modeling, simulation, networked control systems and optimization for power management systems applied to Distributed Generation in AC/DC Microgrids.

**Davor Škrlec** (M'90) is a Full Professor of the University of Zagreb, employed at the Department of Energy and Power Systems, Faculty of Electrical Engineering and Computing. In 1990 he received his M.S. degree and in 1996 his Ph.D. degree in electrical engineering from the University of Zagreb, Faculty of Electrical Engineering and Computing. Research and professional interests include: planning and operation of electrical power networks, distributed energy resources, power systems economics, and geographic information system applications in the power utilities. He has published more than 50 papers from his area of interest and he is author and co-author of several professional books. He is a principal investigator and project leader of several projects funded by industry and government. Core activities within the research activities are focused on optimal planning and operation of active distribution networks and microgrids. He is an active member of IEEE, CIGRE and CIRED.